Confocal Laser Scanning Microscopic Visualization of the Transport of Dextrans After Nasal Administration to Rats: Effects of Absorption Enhancers

Emmeline Marttin,[1] J. Coos Verhoef,[1] Christopher Cullander,[2] Stefan G. Romeijn,[1] J. Fred Nagelkerke,[3] and Frans W. H. M. Merkus[1,4]

Received October 22, 1996; accepted February 18, 1997

Purpose. To visualize the transport pathway(s) of high molecular weight model compounds across rat nasal epithelium *in vivo* using confocal laser scanning microscopy. Furthermore, the influence of nasal absorption enhancers (randomly methylated β-cyclodextrin and sodium taurodihydrofusidate) on this transport was studied.

Methods. Fluorescein isothiocyanate (FITC)-labelled dextrans with a molecular weight of 3,000 or 10,000 Da were administered intranasally to rats. Fifteen minutes after administration the tissue was fixed with Bouin. The nasal septum was surgically removed and stained with Evans Blue protein stain or DiIC18(5) lipid stain prior to visualization with the confocal laser scanning microscope.

Results. Transport of FITC-dextran 3,000 across nasal epithelium occurred via the paracellular pathway. Endocytosis of FITC-dextran 3,000 was also shown. In the presence of randomly methylated β-cyclodextrin 2% (w/v) similar transport pathways for FITC-dextran 3,000 were observed. With sodium taurodihydrofusidate 1% (w/v) the transport route was also paracellular with endocytosis, but cells were swollen and mucus was extruded into the nasal cavity. For FITC-dextran 10,000 hardly any transport was observed without enhancer, or after co-administration with randomly methylated β-cyclodextrin 2% (w/v). Co-administration with sodium taurodihydrofusidate 1% (w/v) resulted in paracellular transport of FITC-dextran 10,000, but morphological changes, i.e. swelling of cells and mucus extrusion, were observed.

Conclusions. Confocal laser scanning microscopy is a suitable approach to visualize the transport pathways of high molecular weight hydrophilic compounds across nasal epithelium, and to study the effects of absorption enhancers on drug transport and cell morphology.

KEY WORDS: confocal laser scanning microscopy; nasal drug delivery; in vivo administration; cyclodextrins; sodium taurodihydrofusidate; fluorescent-labelled dextrans.

[1] Division of Pharmaceutical Technology and Biopharmaceutics, Leiden/Amsterdam Center for Drug Research, Leiden University, P.O. Box 9502, 2300 RA Leiden, The Netherlands.

[2] Departments of Biopharmaceutical Sciences and Pharmaceutical Chemistry, University of California, San Francisco, California.

[3] Division of Toxicology, Leiden/Amsterdam Center for Drug Research, Leiden University, Leiden, The Netherlands.

[4] To whom correspondence should be addressed.

ABBREVIATIONS: CLSM, confocal laser scanning microscopy; DiIC18(5), dioctadecyl indodicarbocyanine; FD3, FITC-dextran 3,000; FD10, FITC-dextran 10,000; FITC, fluorescein isothiocyanate; PBS, phosphate buffered saline; RAMEB, randomly methylated β-cyclodextrin; STDHF, sodium taurodihydrofusidate.

INTRODUCTION

Nasal delivery is a promising alternative for the systemic administration of high potency peptide and protein drugs that are poorly absorbed via the oral route. The nasal cavity is lined with squamous, respiratory and olfactory epithelia. For nasal drug absorption the respiratory portion is most important. The nasal respiratory epithelium is composed of ciliated and non-ciliated columnar cells, goblet cells and basal cells (1). The columnar and goblet cells are found on the apical side of the cell layer, adjacent to the lumen of the nasal cavity. The cilia of the columnar cells transport the mucus secreted by the goblet cells towards the oesophagus by ciliary movement. Basal cells are found adjacent to the basal lamina, at the basolateral side of the epithelium (Fig. 1). Below the basal lamina is the lamina propria, which is rich in blood capillaries. The nasal epithelium has a relatively low transepithelial electrical resistance and a relatively high permeability for large molecules (2–4). Possible transport routes of drugs across the nasal mucosa are transcellular, paracellular and transcytotic (Fig. 1). The absorption barrier for hydrophilic macromolecular compounds is thought to be the intercellular junction i.e., tight junction, and it is suggested (4) that the transport pathway for these substances is paracellular.

The intrinsic nasal bioavailability of polypeptide and protein drugs is low. Absorption enhancers are therefore required for efficient nasal absorption of peptide and protein drugs and to achieve therapeutically relevant plasma concentrations. In the present study randomly methylated β-cyclodextrin (RAMEB) and sodium taurodihydrofusidate (STDHF) were used as enhancers. Methylated β-cyclodextrins have been found to be effective absorption enhancers with a good safety profile, and clinical studies have demonstrated that they are well tolerated in humans (5–7). STDHF has also been shown to have good absorption enhancement properties, but it causes severe local nasal irritation (8,9).

In this study the transport pathways of hydrophilic and high molecular weight model compounds (fluorescent-labelled dextrans of 3,000 Da (FD3) and 10,000 Da (FD10)) across

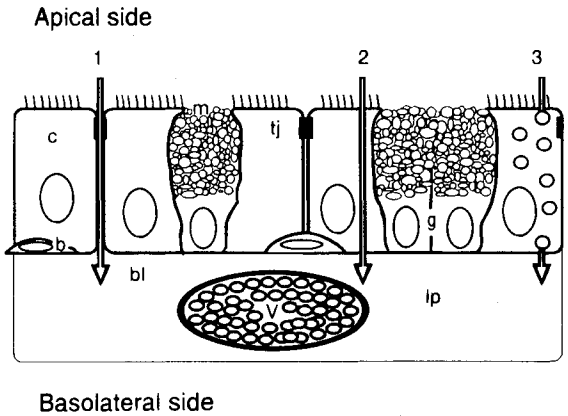

Fig. 1. Schematic representation of transport routes across nasal respiratory epithelium: 1) paracellular; 2) transcellular; 3) transcytotic. Goblet cells (g), ciliated columnar cells (c) and tight junctions (tj) are presented. Basal cells (b) are located on the basal lamina (bl) adjacent to the lamina propria (lp) with blood vessels (v).

0724-8741/97/0500-0631$12.50/0

rat nasal epithelium and the effects of absorption enhancers (RAMEB, STDHF) on this transport were visualized using confocal laser scanning microscopy (CLSM). The nasal absorption was studied *in vivo* by administering FD3 and FD10 intranasally to rats. Fifteen minutes after FD administration with or without absorption enhancer, the tissue was fixed. This survival time was chosen because the absorption maxima of intranasally administered drugs are generally obtained within this time period. After protein or lipid staining, the nasal epithelium was evaluated by CLSM. The advantage of CLSM over conventional fluorescence microscopy is the reduction of out-of-focus fluorescence, resulting in improved resolution and contrast of the micrographs, and the ability of the CLSM to make clearly resolved optical sections of the tissue (10).

MATERIALS AND METHODS

Materials

Dioctadecyl indodicarbocyanine (DiIC18(5)) and aldehyde lysine fixable fluorescein isothiocyanate (FITC)-labelled dextrans of 3,000 and 10,000 Da were obtained from Molecular Probes (Leiden, The Netherlands). Hypnorm (containing 0.315 mg fentanyl citrate and 10 mg fluanisone per mL 0.9% NaCl) was acquired from Janssen Pharmaceutical Ltd. (Oxford, United Kingdom) and Nembutal (sodium pentobarbital, 60 mg/mL) from Sanofi B.V. (Maassluis, The Netherlands). Randomly methylated β-cyclodextrin (RAMEB) was from Wacker (Burghausen, Germany), and sodium taurodihydrofusidate (STDHF) from California Biotechnology Inc. (Mountain View, CA, USA). Formaldehyde solution (extra pure) and paraformaldehyde were obtained from Merck (Darmstadt, Germany), picric acid for microscopy from Fluka A.G. (Buchs, Germany) and acetic acid 98% from Baker (Deventer, The Netherlands). Evans Blue was from ICN Biomedicals Inc. (Aurora, OH, USA). All other reagents were of analytical grade.

Nasal Formulations

The intranasal fluorescent dextran solutions were prepared in physiological saline (0.9% NaCl, w/v). The following formulations were prepared: 0.5% (w/v) FD3; 0.5% (w/v) FD3 with 2% (w/v) RAMEB; 0.5% (w/v) FD3 with 1% (w/v) STDHF; 0.5% (w/v) FD10; 0.5% (w/v) FD10 with 2% (w/v) RAMEB; 0.5% (w/v) FD10 with 1% (w/v) STDHF. Solutions were freshly prepared prior to intranasal application.

Fixatives

Several fixatives were investigated for fixation of the nasal tissue: 4% (w/v) paraformaldehyde dissolved in phosphate buffered saline (PBS) pH 7.4; formaldehyde solution diluted in PBS pH 7.4, formaldehyde: PBS = 1:4 (v/v); 0.2% (w/v) picric acid dissolved in formaldehyde: PBS = 1:4 (v/v); Bouin's fixative, consisting of saturated picric acid: formaldehyde solution: acetic acid = 15:5:1 (v/v/v) (11). All fixatives were freshly prepared before use. After fixation in Bouin, tissue samples were postfixed in formaldehyde: PBS pH 8.0 = 1:4 (v/v).

Intranasal Administration and Tissue Preparation

Male Wistar rats (Broekman Instituut BV, Someren, The Netherlands) were anesthetized with subcutaneous Hypnorm (0.8 mL/kg) and with intraperitoneal Nembutal (0.33 mL/kg). A 5 cm silicone cannula was inserted into the trachea via tracheotomy to enable breathing. A second cannula of 20 cm silicone was inserted via an incision in the oesophagus into the posterior end of the nasal cavity, to perfuse the fixative and to prevent drainage of the formulation from the nasal cavity (via mucociliary clearance). Nasal formulations were administered bilaterally through the nares using a 100 μL syringe with a PVC-tube attached. The tube was inserted at least 0.5 cm into the nostril, and 50 μL per nostril were administered. During dosing and subsequent exposure the rats were supine. Just before the end of the 15 minutes exposure time, the rats were euthanised with an intravenous injection of 0.5 mL Nembutal. All nasal formulations were administered to at least 3 rats.

At 15 minutes after intranasal administration fixation of the tissue was started by flushing the nasal cavity with 5 mL fixative via the oesophageal cannula. The nasal septum was surgically removed and divided in three parts (anterior, medial and posterior). Tissue samples fixed with Bouin were fixed for another 2 h in Bouin and then kept overnight in formaldehyde: PBS pH 8.0 = 1:4 (v/v). Bouin has been shown to be an excellent fixative of nasal morphology, and is preferable above 10% formalin (12). Unfortunately, Bouin can cause more quenching of FD fluorescence than fixation with paraformaldehyde 4% (w/v) or formaldehyde: PBS = 1:4 (v/v) and fluorescence of tissue fixed in Bouin was less bright. Nevertheless, Bouin-fixed tissue samples appeared to be sufficiently bright to be imaged.

Prior to microscopic examination the septum was counterstained 15 minutes with Evans Blue (1%, w/v) or 60 minutes with DiIC18(5) (0.5% w/v dissolved in ethanol:propylene glycol:PBS pH 8.0 = 4:3:1 v/v/v). Evans Blue binds to proteins and can be used to stain respiratory tissue, resulting in red fluorescence (13). The lipophilic stain DiIC18(5) was used for the staining of lipophilic material such as cell membranes, also resulting in red fluorescence (excitation 644 nm, emission 665 nm). For convenience in imaging, the respiratory epithelium was removed from the septum using a scalpel and the tissue was placed directly on the coverslip.

Confocal Laser Scanning Microscopy

A BioRad MRC600 CLSM (BioRad, Hemel Hempstead, UK) specially modified to accommodate both an Argon and a HeNe laser and mounted on a Zeiss IM-35 inverted microscope was used (14). The sample holder consisted of a #1 round coverslip (25 mm diameter and 150 μm thickness, Rofa Mafi, Beverwijk, The Netherlands), a stainless steel ring and a Teflon ring with rubber sealings. The sample holder was assembled by inserting the coverslip into the steel ring and fitting the Teflon ring onto the steel ring and the coverslip. The nasal septum was placed on top of the coverslip. Images were obtained with a Zeiss Planapo 63× oil immersion lens with a numerical aperture of 1.40 or with a Nikon Planapo 60× oil immersion lens, with a numerical aperture of 1.40. FD was excited with the 488 nm line of the Argon laser and Evans Blue with the 633 nm line of the HeNe laser. FD fluorescence was detected using a 515/30 nm band-pass filter, and Evans Blue and DiIC18(5) with a 680/50 nm band-pass filter. The emission filters were from Chroma Technology (Brattleboro, VT, USA). With CLSM, tissue can be scanned in three directions, along

the x-, y-, and z-axes. Optical sections in the horizontal plane were made by scanning in the x and y direction, and sections in the vertical plane were made by scanning one line at different depths in the tissue (x and z direction). BioRad CoMos software was used for image acquisition and analysis. Photoshop (Adobe Systems Inc., Mountain View, CA, USA) was used for reproduction of the micrographs.

RESULTS

Fixation of Nasal Tissue and FD

The nasal respiratory epithelium has a thickness of only two cell layers, and maintaining both the viability and integrity of the drug transport barrier *in situ* requires special provisions such as supply of oxygen and glucose. In pilot experiments, the septum was excised and placed in FD solution in Krebs buffer during CLSM visualization *in situ*. This method resulted in staining of the entire volume of epithelial cells with FD and detection of fluorescence in the lamina propria (results not shown). It seemed that this distribution of fluorescence might be caused by deterioration of tissue during *in situ* FD permeation, as well as by mechanical damage resulting from surgical removal of the septum. To avoid artifacts, FD was administered intranasally *in vivo* to rats. Fifteen minutes after administration the tissue was fixed, and the septum was excised and evaluated by CLSM.

Four fixatives were investigated with respect to their fixation of FD3. After fixation in paraformaldehyde 4% (w/v) in PBS, high fluorescence was observed intracellularly, staining the entire cytoplasm of the cell. The same results were obtained with the fixatives formaldehyde: PBS = 1:4 (v/v) and 0.2% (w/v) picric acid in formaldehyde: PBS = 1:4 (v/v). Finally, Bouin's fixative resulted in fixation of FD3 in the intercellular space, but not in the entire cytoplasm. Autofluorescence was not detected at 515 nm emission, but was weak at 680 nm emission. Evans Blue protein staining and DiIC18(5) lipophilic staining gave bright fluorescence in Bouin-fixated nasal tissue with excitation at 633 nm. There was no cross talk between FD3/FD10 and Evans Blue or DiIC18(5), since Evans Blue and DiIC18(5) were both imaged in the far red wavelength area where FITC did not show any fluorescence.

CLSM Visualization of Protein and Lipophilic Staining in Nasal Epithelium

Vertical cross-sections were made of Bouin-fixed and Evans Blue stained rat nasal respiratory tissue (Fig. 2a). These were compared to images of Bouin-fixed rat nasal tissue embedded in paraffin and stained for mucus with periodic acid Schiff stain (Fig. 2b) (15). The periodic acid Schiff stain was fluorescent, and mucus covering cilia and inside goblet cells could be distinguished. The lamina propria and erythrocytes in blood vessels were also fluorescent. In the vertical optical section certain cells were stained intracellularly with Evans Blue, but only the apical side of the cell was fluorescent (Fig. 2a). The shape and size of Evans Blue stained cells in the optical section were quite similar to those of the goblet cells in the paraffin embedded section (compare Fig. 2a with Fig. 2b), implying that Evans Blue was taken up by mucus inside goblet cells. Apical cells that were not stained intracellularly by Evans Blue

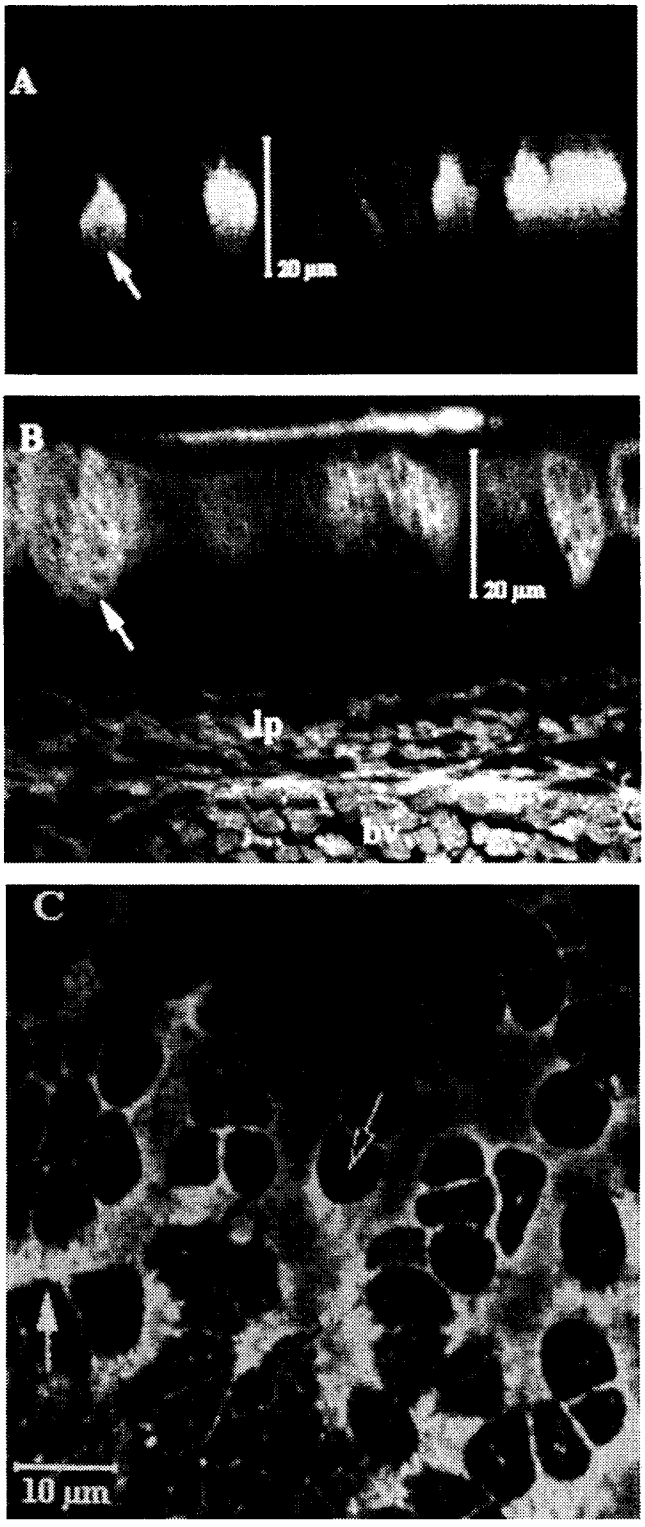

Fig. 2. Rat nasal respiratory epithelium. a) Vertical cross section of Evans Blue protein stained rat nasal tissue, showing goblet cells filled with mucus (closed arrow) and cell membranes between cells; b) Section of rat respiratory epithelium (paraffin embedded coupe) stained for mucosubstances with period acid Schiff stain (15). Mucus is present on the apical side of goblet cells (closed arrow) and also covers columnar cells. Blood vessels (bv) are observed in the lamina propria (lp); c) Horizontal cross section of DiIC18(5) lipid staining of rat nasal respiratory epithelium showing cell membranes, intracellular lipid vesicles (open arrow) and mucus (closed arrow).

were presumably columnar cells. Evans Blue fluorescence was also observed intercellularly, staining the cell membranes between the columnar cells (Fig. 2a).

The lipid stain DiIC18(5) stained the intercellular membranes, and in some cells complete intracellular staining of the cell cross-section was observed (Fig. 2c). The globular shape of the stained part of the cells was comparable to that observed after Evans Blue staining, indicating that DiIC18(5) also stains the mucus in goblet cells. In columnar cells DiIC18(5) was also present intracellularly in spots, staining intracellular vesicles (Fig. 2c). These vesicles were abundant near the apical cell border, but they were also located deeper in the cell.

CLSM Visualization of Nasal FD Transport: Effect of Absorption Enhancers

Fifteen minutes after intranasal administration of FD3, fluorescence was found to be distributed over the larger part of the septum, primarily at the medial and posterior parts where the respiratory epithelium is present. Simultaneous imaging of FD3 and the protein stain Evans Blue showed that the majority of FD3 was located around the respiratory columnar cells, but not between adjacent goblet cells (Fig. 3). FD3 fluorescence was not only located around the cell, but punctate FD3 fluorescence was observed on the apical side of columnar cells. In deeper parts of the cell the spots of FD3 fluorescence were less bright and less abundant. The intracellular punctate FD3 fluorescence was found to be co-localized with fluorescence of DiIC18(5) stained lipid material in the cell (Fig. 3), indicating that FD3 has also been taken up by lipid vesicles. FD3 permeated about 20 to 30 μm into the tissue, which is about one cell layer deep. In the basal cell layer or connective tissue no fluorescence could be detected. From these observations it was concluded that the main transport route of FD3 across the nasal epithelium is paracellular, whereas some intracellular uptake into vesicles has also been shown.

Fifteen minutes after intranasal administration of FD3 with 2% (w/v) of the methylated β-cyclodextrin derivative RAMEB, no differences were observed in the localization and depth of penetration of FD3, in comparison to nasal administration of FD3 without enhancer. In vertical cross-sections of rat nasal epithelium FD3 fluorescence (Fig. 4) was present around columnar cells and goblet cells, but not between goblet cells adjacent to each other. The goblet cells were stained apically by Evans Blue protein stain. Co-localization of FD3 and Evans Blue fluorescence was observed in the mucus layer covering the cells and between cells. A series of horizontal cross sections was made by imaging each successive cross-section 1.9 μm deeper into the tissue (Fig. 5). FD3 fluorescence was observed around cells and as intracellular spots. Occasionally columnar cells were observed in which the intracellular fluorescence distribution was particulate at the apical side of the cell, but more closely packed at the basal side where the cell diameter is decreased. In between goblet cells no FD3 fluorescence was observed. When deeper layers were imaged (e.g. from −7.7 to −13.6 μm; Fig. 5), the fluorescence intensity of FD3 and Evans Blue decreased and no fluorescence could be detected in the basal cell layer or in the basal lamina. Direct quantitative comparison between FD3 penetration without and with RAMEB was not possible, because experimental conditions were different due to Bouin fluorescence quenching. In the presence of RAMEB the major transport route of FD3 across the nasal epithelium was paracellular, in combination with vesicular uptake intracellularly.

Fifteen minutes after nasal administration of FD10 the penetration of this macromolecular compound into the nasal epithelium appeared to be negligible without absorption enhancer. In a vertical cross-section FD10 fluorescence could only be observed in the mucus layer on top of the cells, but not between the cells or intracellularly (Fig. 6). Nasal instillation of FD10 with RAMEB (2%, w/v) resulted in similar images.

After nasal administration of FD3 or FD10 with the fusidate derivative STDHF (1%, w/v) both paracellular transport and intracellular punctate uptake of FD fluorescence were

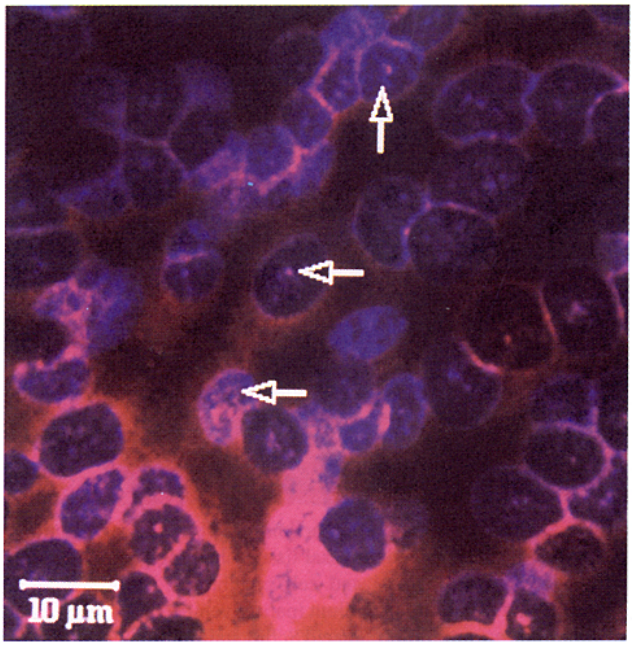

Fig. 3. Horizontal cross section of the transport of FD3 across the rat nasal respiratory epithelium, showing FD3 transport (blue) and DiIC18(5) lipophilic staining (red), as well as co-localization of FD3 and protein staining (purple). Intracellular particulate FD3 and lipophilic staining (open arrows) is indicative of endocytotic FD3 uptake.

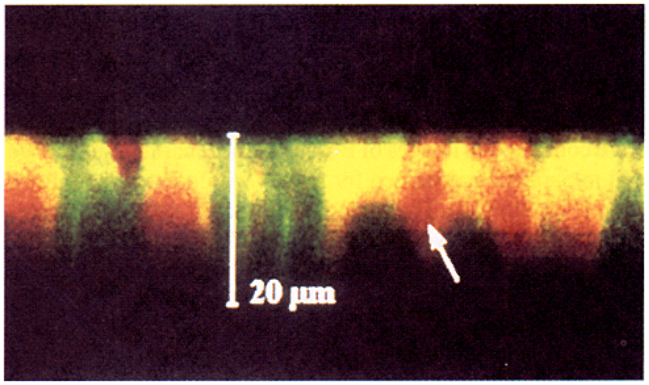

Fig. 4. FD3 transport pathways across rat nasal respiratory epithelium in the presence of RAMEB (2%, w/v). Vertical cross section of FD3 transport (green) and Evans Blue protein staining (red), as well as co-localization of FD3 and protein staining (yellow). Mucus is indicated by a closed arrow.

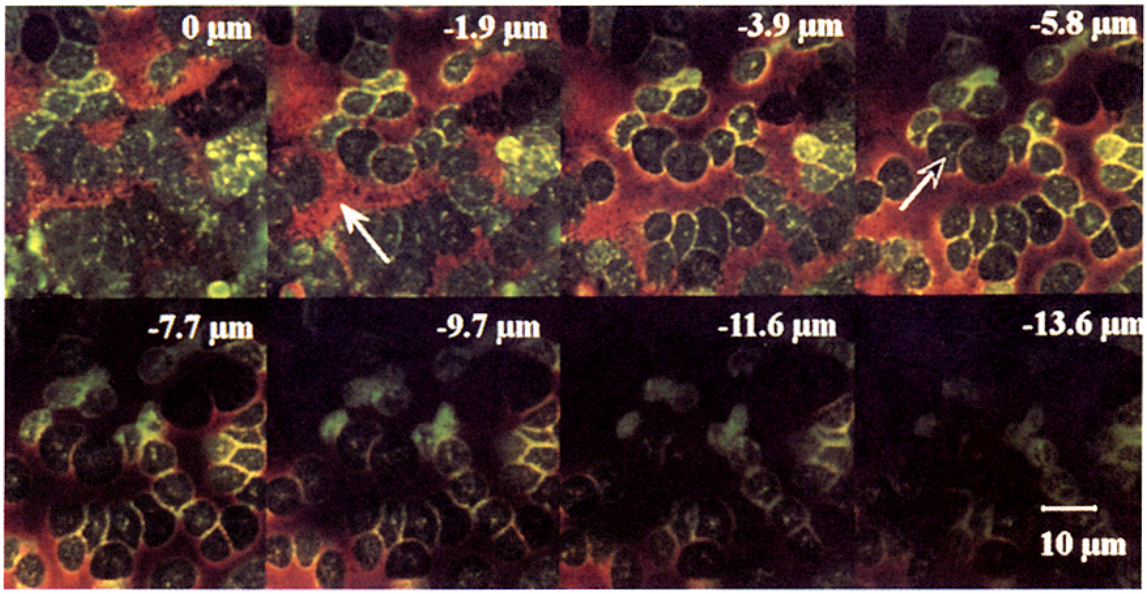

Fig. 5. FD3 transport pathways across rat nasal respiratory epithelium in the presence of RAMEB (2%, w/v). Series of 8 horizontal cross-sections from 0 µm to −13.6 µm, taken with steps of 1.9 µm thickness. FD3 fluorescence is green, Evans Blue protein staining is red, and co-localization of FD3 and Evans Blue is yellow. Closed arrow indicates goblet cell with mucus (red) and the open arrow endocytotic uptake of FD3 (yellow). In deeper layers the fluorescence intensity was remarkably decreased.

observed (see Fig. 7). After intranasal STDHF administration Evans Blue protein staining of mucus could not be detected intracellularly. This is indicative of mucus extrusion, which resulted in a layer of mucus covering the apical cell layer. The appearance of extruded mucus was flocculent and FD10 was found to be present in the mucus layer (Fig. 7). The cells were larger than after FD administration without any enhancer or with RAMEB 2% (compare Fig. 7 with Fig. 3). Since the majority of the nasal respiratory cells were swollen, it is likely that goblet as well as columnar cells were affected. The nasal permeation of FD3 in the presence of STDHF was comparable to that of FD10 with STDHF, both with respect to transport pathways and morphological changes.

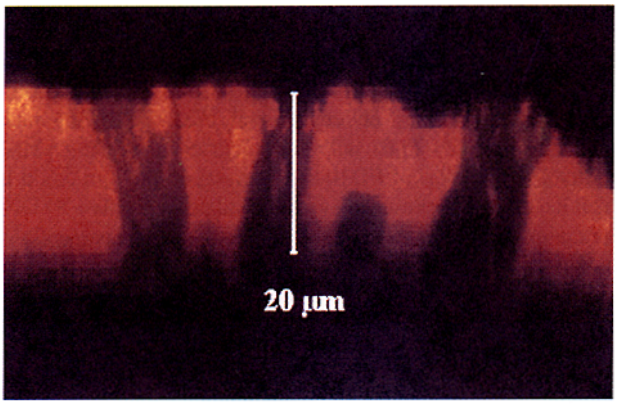

Fig. 6. Vertical cross section of FD10 permeation in rat nasal respiratory epithelium. There was hardly any FD10 fluorescence (green) present. Goblet cells were visible (Evans Blue protein staining, red) and co-localization of FD10 and Evans Blue protein stain (yellow) was present in the mucus layer covering the apical side of the cell-layer.

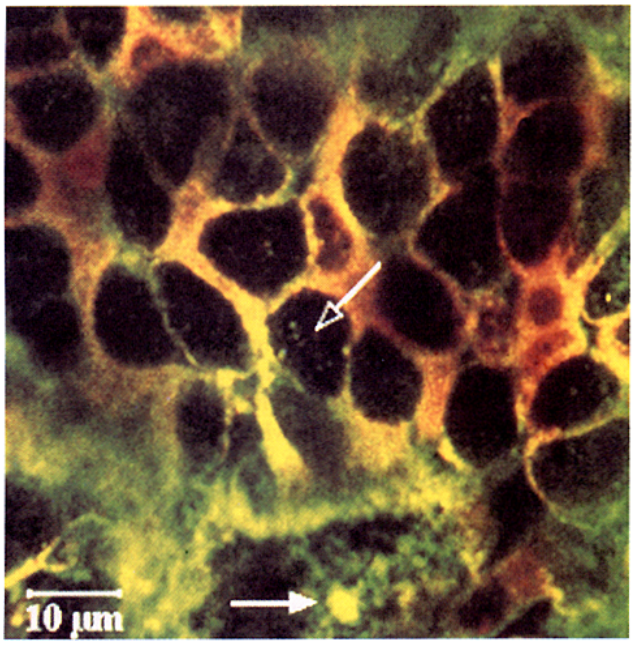

Fig. 7. Horizontal cross section of FD10 transport pathways with STDHF (1%, w/v) across nasal respiratory epithelium. FD10 (green) was present around cells and intracellularly (open arrow). Evans Blue protein staining is red, and co-localization of FD10 and Evans Blue protein staining is yellow. Within the goblet cells mucus could not be detected anymore, and the mucus extruded from these cells was visible (closed arrow). Columnar and extruded goblet cells were swollen; in comparison with Fig. 3, most cells were almost doubled in size.

DISCUSSION

Bouin was found to be the only fixative that resulted in good fixation of nasal respiratory epithelium and FD3, because FD was present in the intercellular space, but not in the entire cytoplasm. The *in vivo* fixation of nasal respiratory tissue and aldehyde-fixable FITC-labelled dextrans was therefore possible using Bouin. With this procedure the transport of high molecular weight dextrans after intranasal administration *in vivo* can be visualized. While FD3 could only be detected near the tissue surface, the transport pathway(s) through the apical cell layer were readily visualized. It is not clear whether the limited depth of FD visualization is due to absorption and/or scattering of emitted fluorescence, or because there were smaller amounts of fluorophore in this deeper part of the tissue.

The simultaneous imaging of FD transport and the protein-staining Evans Blue or lipid-staining DiIC18(5) made it possible to obtain insights into the mechanisms of transport. The present CLSM visualization studies of FD3 transport across the nasal epithelium of rats indicate that a major transport pathway of this high molecular weight compound is paracellular. FD3 was transported paracellularly between columnar cells and between columnar and goblet cells, but not between adjacent goblet cells. The lack of FD3 penetration between goblet cells might be explained by the lipophilic components of the goblet cells (16), which were stained by the lipophilic stain DiIC18(5). This lipophilic nature might hinder the permeation of the hydrophilic FD3 in between goblet cells. FD3 was not only transported paracellulary, it was also taken up by the cells in vesicles, as indicated by co-localization of DiIC18(5) staining and FD3-containing intracellular spots. The uptake of macromolecules into intracellular vesicles has been observed in a number of electron microscopic studies (17–19). These studies suggest that the visualization of FD3 intracellularly in spots, as shown in the present study, is most likely due to endocytotic uptake of the dextran molecules. The reported uptake of human growth hormone in ciliated rabbit nasal tissue probably took place via endocytotic vesicles at the apical side of the cytoplasm (17). For rat nasal epithelium, it has been demonstrated that horseradish peroxidase was taken up by vesicles at the apical side of the ciliated cells (18). In guinea pig tracheal tissue horseradish peroxidase and ferritin were found in vesicles near the apical cell border at 5 and 15 minutes after intratracheal administration. After 40 minutes these vesicles were also localized in a more basal position in the cells (19). Because the basal cells and the lamina propria could not be visualized in the present CLSM studies, it cannot be ascertained whether transcytosis of FD3 also occurred.

No qualitative or quantitative differences in nasal transport routes of FD3 with or without the β-cyclodextrin derivative RAMEB could be observed. However, in an absorption study in rats it was found that 40% of the intranasal dose of a dextran of 3400 Da was absorbed (without absorption enhancer), indicating that dextrans of this size are absorbed intranasally to a large extent (3). With CLSM it is not possible to obtain such quantitative data. Nevertheless, RAMEB has been reported to substantially increase nasal absorption of calcitonin (MW 3,300) in rats *in vivo* (6). After intranasal administration of FD10 only negligible amounts of this compound were present intercellularly or in intracellular vesicles, both without any enhancer and with RAMEB as absorption enhancer. The difference in transport of FD3 and FD10 across the rat nasal epithelium without enhancers has also been demonstrated previously. For a small dextran of 3400 Da about 40% of the nasally administered dose was absorbed, whereas of larger dextrans of 9060–9800 Da only 2.7 to 6.4% of the dose was absorbed (3).

In the present study, CLSM visualization of nasal epithelial transport of FD3 and FD10 in the presence of STDHF (1%, w/v) shows transport of both dextrans taking place primarily via the paracellular pathway, although endocytotic uptake also occurs. In another CLSM study with Caco2-cell monolayers it has been demonstrated that the transport pathways of 4 kDa FITC-labelled dextrans with STDHF were both paracellular and transcellular (20). In the present study it was observed that STDHF resulted in mucus extrusion from the goblet cells and swelling of both goblet and columnar cells. This swelling might partly be caused by the expansion of the apical part of goblet cells when mucus is extruded from these cells. The process of mucus extrusion takes place by swelling of the intracellular mucin granules prior to exocytosis in the extracellular space (16). The enlargement of the cells might also be caused by toxic effects of STDHF on respiratory columnar and goblet cells. Since STDHF resulted in morphological changes of the nasal epithelium, the differences between STDHF and RAMEB with respect to their enhancement of nasal FD10 transport are most likely due to the effects of STDHF on nasal epithelial cell morphology. In previous histological studies on the effects of STDHF on rat nasal epithelium, both mucus extrusion and morphological alterations of nasal respiratory cells were reported (21,22). Moreover, STDHF also caused significant release of proteins and intracellular enzymes from rat nasal epithelium at 15 minutes after nasal administration, indicating that severe cell damage occurred (23). The intranasal tolerability of STDHF in man is low, since it has been shown to display severe irritation prohibitive of further clinical investigation (9).

In conclusion, Bouin fixation of FD administered intranasally to rats *in vivo* has proven to be a suitable method to visualize transport routes of hydrophilic macromolecular compounds in nasal epithelium with CLSM. For FD3 a major transport route 15 minutes after intranasal administration in rats is paracellular, particularly around columnar cells, but not around goblet cells. Endocytotic uptake of FD3 also occurs, but it is not clear whether this endocytotic process is followed by transcytotic transport of FD3. In the presence of the β-cyclodextrin derivative RAMEB paracellular transport is also predominant, accompanied by endocytosis of FD3. Following nasal administration of FD10 without enhancer or with RAMEB hardly any transport of FD10 across nasal epithelium could be visualized. In the presence of the fusidate derivative STDHF the major transport route of both FD3 and FD10 is paracellular, and also endocytosis of FD3 and FD10 occurs. However, intranasal administration of STDHF results in morphological changes, indicating that STDHF damages the nasal epithelium.

ACKNOWLEDGMENTS

Financial support of this study by the Ministry of Health of the Netherlands is gratefully acknowledged. Dr. Cullander's

contribution was partially supported by NIH. The technical assistance of Hans de Bont was greatly appreciated.

REFERENCES

1. N. A. Monteiro-Riviere and J. A. Popp. *Am. J. Anat.* **169**:31–43 (1984).
2. K. I. Hosoya, H. Kubo, H. Natsume, K. Sugibayashi, Y. Morimoto, and S. Yamashita. *Biopharm. Drug Disp.* **14**:685–696 (1993).
3. A. N. Fisher, L. Illum, S. S. Davis, and E. H. Schacht. *J. Pharm. Pharmacol.* **44**:550–554 (1992).
4. C. McMartin, L. E. F. Hutchinson, R. Hyde, and G. E. Peters. *J. Pharm. Sci.* **76**:535–540 (1987).
5. W. A. J. J. Hermens, C. W. J. Belder, J. M. W. M. Merkus, P. M. Hooymans, J. Verhoef, and F. W. H. M. Merkus. *Eur. J. Obs. Gynecol. Reprod. Biol.* **40**:35–41 (1991).
6. N. G. M. Schipper, J. C. Verhoef, S. G. Romeijn, and F. W. H. M. Merkus. *Calcif. Tissue Int.* **56**:280–282 (1995).
7. K. Matsubara, K. Abe, T. Irie, and K. Uekama. *J. Pharm. Sci.* **84**:1295–1300 (1995).
8. P. A. Baldwin, C. K. Klingbeil, C. J. Grimm, and J. P. Longenecker. *Pharm. Res.* **7**:547–552 (1990).
9. T. Kissel, J. Drewe, S. Bantle, A. Rummelt, and C. Beglinger. *Pharm. Res.* **9**:52–57 (1992).
10. Y. Rojanasakul, S. W. Paddock, and J. R. Robinson. *Int. J. Pharm.* **61**:163–172 (1990).
11. R. Bacallao, K. Kiai, and L. Jesaitis. In J. B. Pawley (ed.), *Handbook of biological confocal microscopy*, Plenum Press, New York and London, 1995, pp. 311–325.
12. L. C. Uraih and R. R. Maronpot. *Environ. Health Persp.* **85**:187–208 (1990).
13. A. Saria and J. M. Lundberg. *J. Neurosci. Meth.* **8**:41–49 (1983).
14. J. F. Nagelkerke and H. J. G. M. De Bont. *J. Micros.* **184**:58–61 (1996).
15. E. Marttin, J. C. Verhoef, S. G. Romeijn, P. Zwart, and F. W. H. M. Merkus. *Int. J. Pharm.* **141**:151–160 (1996).
16. P. Verdugo. *Annu. Rev. Physiol.* **52**:157–176 (1990).
17. C. Agerholm, L. Bastholm, P. B. Johansen, M. H. Nielsen, and F. Elling. *J. Pharm. Sci.* **83**:618–663 (1994).
18. S. Y. Jeon, N. J. Kim, E. G. Hwang, S. K. Hong, and Y. G. Min. *Ann. Otol. Rhinol. Laryngol.* **104**:895–898 (1995).
19. J. Richardson, T. Bouchard, and C. C. Ferguson. *Lab. Invest.* **35**:307–314 (1976).
20. M. A. Hurni, A. B. Noach, M. C. M. Blom-Rosmalen, A. G. De Boer, J. F. Nagelkerke, and D. D. Breimer. *J. Pharmacol. Ex. Ther.* **267**:942–950 (1993).
21. S. G. Chandler, L. Illum, and N. W. Thomas. *Int. J. Pharm.* **76**:61–70 (1991).
22. R. D. Ennis, L. Borden, and W. A. Lee. *Pharm. Res.* **7**:468–475 (1990).
23. E. Marttin, J. C. Verhoef, S. G. Romeijn, and F. W. H. M. Merkus. *Pharm. Res.* **12**:1151–1157 (1995).